



RESEARCH PAPER

 OPEN ACCESS 

Early oseltamivir reduces risk for influenza-associated aspergillosis in a double-hit murine model

Laura Seldeslachts ^a, Lore Vanderbeke^b, Astrid Fremau^a, Agustin Reséndiz-Sharpe^b, Cato Jacobs^c, Bo Laeveren^a, Tessa Ostyn^a, Lieve Naesens^d, Matthias Brock^e, Frank L. Van De Veerdonk^f, Stephanie Humblet-Baron^g, Erik Verbeke^h, Katrien Lagrou^b, Joost Wauters^{c*} and Greetje Vande Velde ^{a*}

^aDepartment of Imaging and Pathology, Biomedical MRI unit/MoSAIC, Ku Leuven, Leuven, Belgium; ^bDepartment of Microbiology, Immunology and Transplantation, Laboratory of Clinical Bacteriology and Mycology, Ku Leuven, Leuven, Belgium; ^cDepartment of Microbiology, Immunology and Transplantation, Laboratory for Clinical Infectious and Inflammatory Disorders, Ku Leuven, Leuven, Belgium; ^dDepartment of Microbiology, Immunology and Transplantation, Laboratory of Virology and Chemotherapy (Rega Institute), Ku Leuven, Leuven, Belgium; ^eFungal Biology Group, School of Life Sciences, University of Nottingham, Nottingham, UK; ^fDepartment of Internal Medicine, Radboud University Medical Center, Nijmegen, Netherlands; ^gDepartment of Microbiology, Immunology and Transplantation, Laboratory of Adaptive Immunity, Ku Leuven, Leuven, Belgium; ^hDepartment of Imaging and Pathology, Ku Leuven, Leuven, Belgium

ABSTRACT

Invasive pulmonary aspergillosis (IPA) is a life-threatening fungal infection occurring mainly in immunocompromised patients. We recently identified IPA as an emerging co-infection with high mortality in critically ill, but otherwise immunocompetent influenza patients. The neuraminidase inhibitor oseltamivir is the current standard-of-care treatment in hospitalized influenza patients; however, its efficacy in influenza-associated pulmonary aspergillosis (IAPA) is not known. Therefore, we have established an imaging-supported double-hit mouse model to investigate the therapeutic effect of oseltamivir on the development of IPA. Immunocompetent mice received intranasal instillation influenza A or PBS followed by orotracheal inoculation with *Aspergillus fumigatus* 4 days later. Oseltamivir treatment or placebo was started at day 0, day 2, or day 4. Daily monitoring included micro-computed tomography and bioluminescence imaging of pneumonia and fungal burden. Non-invasive biomarkers were complemented with imaging, molecular, immunological, and pathological analysis. Influenza virus-infected immunocompetent mice developed proven airway IPA upon co-infection with *Aspergillus fumigatus*, whereas non-influenza-infected mice fully cleared *Aspergillus*, confirming influenza as a risk factor for developing IPA. Longitudinal micro-CT showed pulmonary lesions after influenza infection worsening after *Aspergillus* co-infection, congruent with bioluminescence imaging and histology confirming *Aspergillus* pneumonia. Early oseltamivir treatment prevented severe influenza pneumonia and mitigated the development of IPA and associated mortality. A time-dependent treatment effect was consistently observed with imaging, molecular, and pathological analyses. Hence, our findings underscore the importance of initiating oseltamivir as soon as possible, to suppress influenza infection and mitigate the risk of potentially lethal IAPA disease.

ARTICLE HISTORY

Received 15 January 2021
Revised 9 July 2021
Accepted 25 August 2021

KEYWORDS

influenza-associated pulmonary aspergillosis; oseltamivir; multimodal preclinical imaging-supported mouse model; *Aspergillus fumigatus*; Influenza

Introduction


Invasive pulmonary aspergillosis (IPA) is a life-threatening fungal infection characterized by acute infection of the lungs occurring mainly in immunocompromised patients [1]. In the last decade, severe influenza has gained a foothold worldwide as an emerging risk factor for IPA [1,2]. Recently, we published two retrospective case-control studies on influenza-associated pulmonary aspergillosis (IAPA) [1,3]. IPA was found as a co-infection in 19% of patients with severe influenza at a median of 3 days

after intensive care unit (ICU) admission [1]. Remarkably, the cohort of co-infected patients had a high mortality risk of 51%, whereas that of severe influenza without IAPA was 28% [1]. By June 2018, 128 IAPA cases were published, with 28% of the patients having no underlying medical condition [4]. These incidence rates emphasize the importance of recognizing influenza as an independent risk factor for IPA and the high morbidity and mortality associated with it. Hence, an international group of experts has published a case definition of IAPA to

CONTACT Greetje Vande Velde  greetje.vandevelde@kuleuven.be

#Co-first author

*Co-last author

 Supplemental data for this article can be accessed [here](#).

© 2021 The Author(s). Published by Informa UK Limited, trading as Taylor & Francis Group.

This is an Open Access article distributed under the terms of the Creative Commons Attribution-NonCommercial License (<http://creativecommons.org/licenses/by-nc/4.0/>), which permits unrestricted non-commercial use, distribution, and reproduction in any medium, provided the original work is properly cited.

facilitate research in epidemiology, diagnosis, and management of this emerging disease [5].

Globally, influenza is estimated to affect 5–10% of the population each year. On average, 3–5 million cases of severe influenza occur annually worldwide, leading to 290,000–650,000 deaths [6,7]. Virus-induced lung epithelial damage and host immune response aberrations are hallmark manifestations of severe influenza infection [8–11]. These pathological processes are the key to success for secondary pathogenic microorganisms to enter the lung parenchyma and colonize patients [12]. Bacterial superinfections with *Staphylococcus aureus* and *Streptococcus pneumoniae* are well-defined complications of a severe influenza infection and different mouse models of influenza-bacterial-co-infection have been developed [13–16]. However, until today, influenza-associated fungal co-infection models are not yet widely experimentally addressed. To preclinically assess potential treatment strategies, a robust animal model recapitulating IAPA disease in humans is needed.

Currently, the neuraminidase inhibitor (NAI) oseltamivir, is the standard-of-care to suppress influenza. This drug prevents successful virus replication by inhibiting the viral neuraminidase. Several clinical studies have corroborated that early oseltamivir treatment improves the outcome in critically ill patients suffering from influenza [17–19]. Also in mice, oseltamivir is known to improve survival, body weight loss, and to reduce viral lung titers, thereby limiting the severity of lung damage [20,21]. In addition, in a mouse model of influenza-bacterial-co-infection both prophylactic and early oseltamivir treatments improved the survival and reduced the extent of the secondary pneumococcal pneumonia [22–24]. Likewise, we hypothesize that oseltamivir may reduce the susceptibility to IAPA in mice and men through attenuation of influenza infection.

Here, we establish a double-hit mouse model for IAPA and report on its imaging capabilities to longitudinally follow-up influenza pneumonia and exacerbation after challenge with *A. fumigatus* conidia. In this model, we assessed whether IAPA is prevented by oseltamivir treatment initiated at different time points during influenza infection.

Materials and methods

Influenza virus strain

A mouse-adapted influenza virus A/H3N2/Ishikawa/7/82 was kindly provided as a mouse lung homogenate by M. Hosoya (Fukushima, Japan) [25]. The virus was expanded in Madin–Darby canine kidney (MDCK)

cells, which were also used to determine the virus titer by standard plaque assay. Original virus stocks were thawed and diluted to a final concentration of 500 PFU/mL.

Aspergillus strain

In all experiments, an *A. fumigatus* derivative of strain CBS144.89 expressing a red-shifted thermostable firefly luciferase from the *akuB* locus was used. In brief, a codon-optimized red-shifted and thermostable firefly luciferase (*luc*_{OPT_red_TS}, GenBank accession number: MT554554) was synthesized (GenScript) and cloned under control of the 820 bp promoter of the glyceraldehyde-3-phosphate dehydrogenase (*gpdA*) from *Aspergillus nidulans* and fused with a 322 bp *gpdA* terminator region. This luciferase expression construct was cloned into the *ptrA*-pJET1 plasmid [26] containing the pyrithiamine resistance gene. The entire 4785 reporter-*ptrA* cassette was amplified with oligonucleotides P*gpdAIFKu80up_f* (5' – CCC TGA GGC GGC CGC GGG CTG AGT AAT AAG – 3') and *ptrAIFKu80do_r* (5' – AAC TTT GGG CGG CCG CGT ATT ATA CTG TC – 3') to allow subsequent *in vitro* recombination with the upstream and downstream flanking regions of the *akuB* gene from *A. fumigatus*. Genomic DNA of the *A. fumigatus* wild-type strain CBS144.89 served as template for amplification of the 819 bp upstream and 666 bp downstream region of the *akuB* gene. The *akuB* upstream region was amplified with oligonucleotides *KU80upIFpUC_f* (5' – CGA GCT CGG TAC CCG GGA CTC AAT TTC TAT TCT AGA GCA TC- 3') and *KU80upIFP*gpdA_r** (5' – GCGGCCGCTCAGGGTTCGTCAAAGTCAGTAC – 3'). The downstream region was amplified with oligonucleotides *KU80doIF*ptrA_f** (5' – GCG GCC GCC CAA AGT TAA AGG GCG CAA GC) and *KU80doIFpUC_r* (5' – CTC TAG AGG ATC CCC GGG CTA TCA CTT TGC CCA GTC – 3'). A pUC19 plasmid was linearized with *Sma*I and the three PCR products were assembled with the plasmid by *in vitro* recombination using the InFusion HD cloning kit (Takara/Clontech). Assembled plasmids were amplified in *Escherichia coli* DH5α. After isolation of the plasmid (NucleoSpin plasmid, Machery-Nagel) the entire cassette was excised from the plasmid backbone by *Sma*I restriction and used for protoplast transformation of the *A. fumigatus* wild-type strain CBS144.89 using 0.1 μg pyrithiamine/ml (Sigma) as selection marker. Transformants were pre-screened by cultivation on *Aspergillus* minimal medium [27] containing 0.2 mM D-luciferin (Promega) and imaging of plates in

a Chemi Doc XRS system (BioRad) under chemiluminescent setting. Selected transformants were analyzed for single copy integration of the reporter construct into the *akuB* locus and strain Af_Δ*akuB*::*luc*_{OPT_red_TS_ptrA} No. 5 was selected for further use. For preparation of conidia suspensions, the strain was cultured on Sabouraud agar for 3 days at 42°C. *A. fumigatus* conidia were harvested by detaching with NaCl-0.1% Tween 80 (Sigma-Aldrich, Diegem, Belgium) solution, followed by vigorous shaking and filtering of the suspension. Finally, spores were counted with a Neubauer hemocytometer and diluted to a final concentration of 5×10^9 conidia/mL.

Mouse model

All animal experiments were approved by the KU Leuven Ethical Committee for animal research (license p074/2018). Eight to ten weeks old immunocompetent male C57BL/6NTac mice (internal stock of the Laboratory Animal Center, KU Leuven) were kept in a conventional animal facility in individually ventilated cages with free access to food and water. To prevent bacterial infection, an antibiotic (50 mg/kg/day, Baytril®, Bayer) was added to the drinking water. Animals were randomly assigned to experimental groups. Mice received intranasal instillation of 10 plaque forming units (PFU) influenza virus or PBS (10 µL per nostril) under inhalation anesthesia with isoflurane (1.5–2% in oxygen, Primal Critical Care). Mice were orotracheally inoculated with 20 µL of *A. fumigatus* spore solution under injection anesthesia (Ketamine (75 µg/g) and Medetomidine (1 µg/g)) (Figure 1(a)) or isoflurane (Figure 2a, Figure 4a). Oseltamivir (10 mg/kg) or PBS treatment was administered twice daily by oral gavage. During the experiments, mice were monitored daily for body weight, general condition, and respiratory parameters, non-invasively scanned with micro-computed tomography and bioluminescence imaging and sacrificed when the humane or predefined experimental endpoint was reached, by an overdose of pentobarbital via intraperitoneal injection [28]. Subsequently, blood was drawn by cardiac puncture, bronchoalveolar lavage (BAL) fluid was obtained by three lung lavages with 700 µL 0.9% NaCl and right lung lobes were aseptically collected, weighted, and homogenized in PBS. The left lung was inflated with 400 µL 10%-formalin, 24 h post fixated and then stored in PBS-0.1% sodium-azide at 4°C. Subsequently, histopathology analysis was performed. BAL and blood were centrifuged at respectively 1000 x g for 10 min at 4°C and 13,817 x g for 4 min at 4°C. BAL supernatant, serum and lung homogenates were

used for further quantification of virus titers, fungal burden, and cytokine analysis.

Micro-computed tomography (µCT)

A dedicated whole-body small animal µCT scanner (SkyScan 1278, Bruker micro-CT, Kontich, Belgium) was used to acquire lung µCT data of free-breathing anesthetized (isoflurane, 1.5–2% in oxygen, Piramal Critical Care) animals in supine position. Following scan parameters were used: 50 kVp X-ray source, 1 mm aluminum X-ray filter, 350 µA current and 150 ms exposure time per projection acquiring projections with 0.9° increments over a total angle of 220°. Acquisition resulted in respiratory weighted reconstructed 3D dataset with isotropic voxel size of 50 µm in a total scanning time of 3 min, associated with a radiation dose exposure of 69–89 mGy [29]. Temperature, respiration rate, and visual information were used to monitor mice while scanning. µCT data was reconstructed, visualized, and processed using NRecon, DataViewer, and CTan software, provided by the manufacturer. Reconstruction parameters were: smoothing 2, beam hardening correction of 10%; post alignment and ring artifact reduction were optimized for each individual scan. µCT data were processed and calibrated to Hounsfield units (HU) as described before [30]. In brief, regions of interests (ROI), resulting in a volume of interest (VOI) covering the entire lung, were manually delineated on transverse images, thereby avoiding the heart and main blood vessels [30,31]. Subsequently, imaging-derived biomarkers of lung pathology (total lung volume (TLV), aerated lung volume (ALV), non-aerated lung volume (NALV) and mean lung densities) were quantified. To distinguish ALV from NALV, a fixed manually set threshold of 94 HU was used based on histogram in CTan (TLV ranges from –1000 to 1160, ALV from –1000 to (–94), NALV –85 to 1160). Visual observations of transverse µCT images were semi-quantitatively scored by two blinded researchers (LS and BL) according to [31] with minor modifications. In brief, four transverse images at different, defined positions in the lung were selected for each animal at each time point on the reconstructed µCT. Per animal, a score of zero was assigned to each image at baseline. Subsequently, scores of +0.25, 0 or –0.25 depending on observed worsening, stabilization, or improvement of pulmonary lesions (pulmonary infiltrate), respectively, were assigned and added to the score of the previous day to obtain a cumulative score.

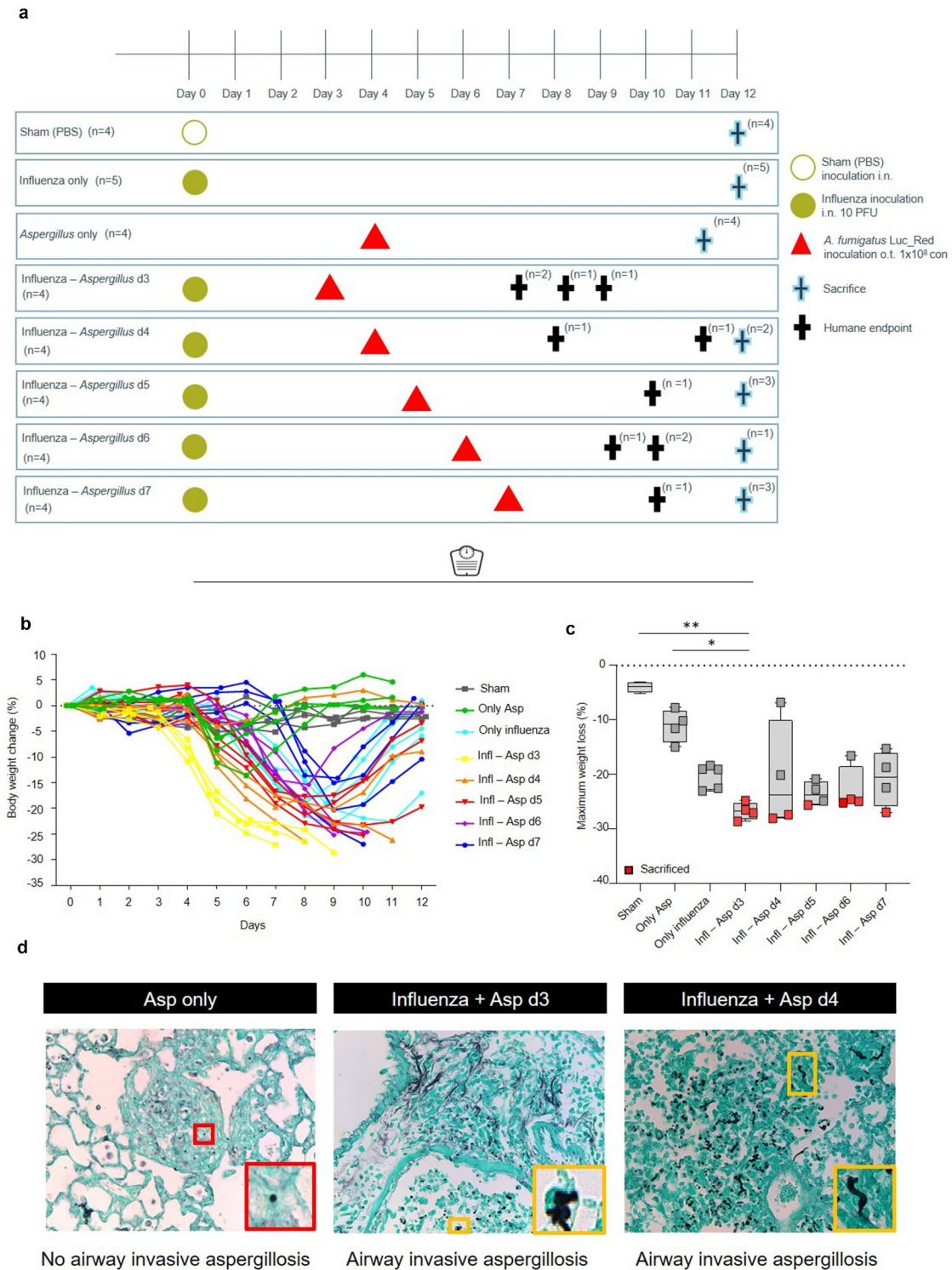


Figure 1. Second-hit with *A. fumigatus* during active influenza infection drives risk for clinical deterioration with IPA. (a) experimental setup for the development of double-hit mouse model: immunocompetent mice received influenza A virus on day 0, followed by orotracheal inoculation with *A. fumigatus* conidia on day 3, 4, 5, 6 or day 7 post-influenza infection. control groups of mock-infected (sham), influenza only and *aspergillus* only were included. body weight was measured daily. (b) body weight evolution of sham-infected and infected mice. (c) maximum body weight loss per animal for different experimental arms. red box represents mice which were sacrificed because humane endpoints were reached (d) grocott's methenamine silver staining of left lungs from mice with *A. fumigatus*, influenza-*A. fumigatus* day 3 co-infected, influenza-*A. fumigatus* day 4 co-infected mice sacrificed at respectively day 7 and day 8 post influenza infection (magnification $\times 400$). *Aspergillus* conidia (red box) and hyphae (yellow box).

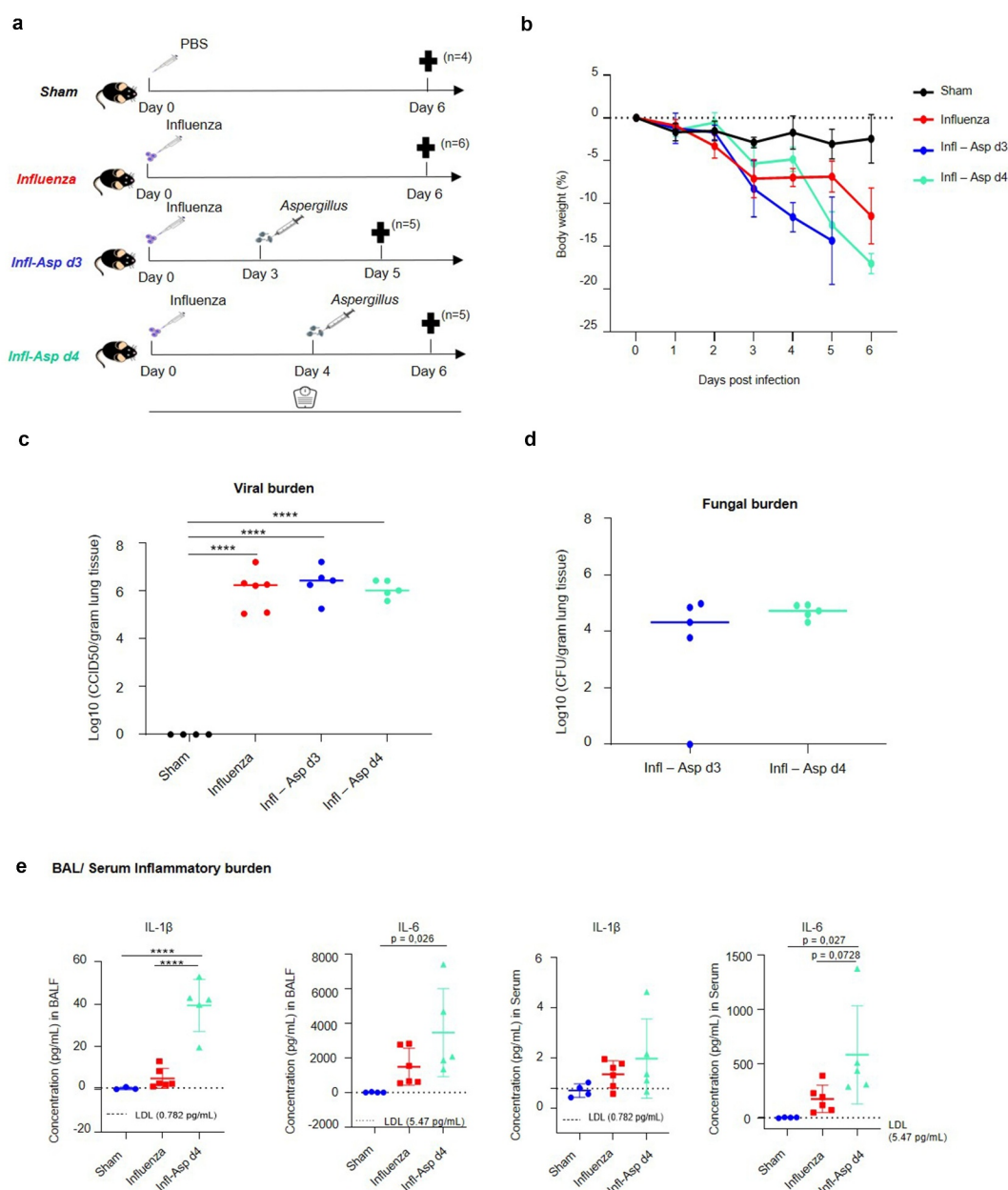


Figure 2. Immunocompetent mice develop IPA in a background of a sublethal influenza-pneumonia. (a) experimental setup: immunocompetent mice received influenza A virus on day 0 followed by orotracheal inoculation with *A. fumigatus* conidia on day 3 and 4 post-influenza infection. sacrifice was performed 2 days after co-infection. Single control groups of either mock infected (sham) and influenza alone with sacrifice on day 6 were included. (b) body weight evolution of immunocompetent mice infected with influenza on baseline (day 0) and co-infected with *a. fumigatus* 3 or 4 days later. Parallel sham-infected and influenza-infected mice were included as controls. (c) graph representing the log₁₀ CCID50 per gram lung tissue from sham-infected (sacrificed on d6), influenza-infected (sacrificed on d6), influenza – *A. fumigatus* day 3 (sacrificed on d5) and influenza-*A. fumigatus* day 4 co-infected mice (sacrificed on d6). (d) Log₁₀ colony forming unit (CFU) count per gram lung tissue from influenza-*A. fumigatus* day 3 (sacrifice d5) and influenza-*A. fumigatus* day 4 co-infected mice (sacrifice d6). (e) Scatter plot of cytokine response (IL-1 β and IL-6) in serum and bronchoalveolar lavage fluid (BALF) of mock infected (sham), influenza infected and influenza-*Aspergillus* day 4 co-infected mice sacrifice on day 6. dashed line represents lower detection limit of the standards (LDL). In influenza-*A. fumigatus* day 4 co-infected mice. all graphs are represented as mean or as mean \pm SD, **** $P < 0.0001$.

Bioluminescence imaging (BLI)

For *in vivo* BLI, the mice were intraperitoneally injected with D-luciferin (in PBS, 50 mg/mL, 500 mg/kg), then

anesthetized (isoflurane inhalation, 1.5–2% in oxygen, Piramal Critical Care) and placed in supine position in an IVIS Spectrum System (Perkin-Elmer, Hopkinton, MA, USA). Five consecutive images were acquired

starting 10 min after injection. Following settings were used: exposure time of 1 min, medium binning, F/stop of 1 and subject height of 1.5 cm. Quantification of BLI data reflecting fungal lung burden was performed with software provided by the manufacturer (Living Image Software version 4.7.3). Total photon flux (p/s) was measured through a ROI of 6.9 cm², covering the lungs, and the maximum from consecutive acquisitions used for further analysis.

For *ex vivo* BLI, 1:5 serial dilutions of homogenized right lung lobes in black 96-well plates (Nunc® Microwell, Thermo Fisher Scientific, Merelbeke, Belgium) were placed in the IVIS Spectrum after addition of 10% D-luciferin (in PBS, 50 mg/mL). Images were acquired until maximum signal intensity was reached with following settings: exposure time of 1 min per image, medium binning, F/stop of 1 and subject height of 1 cm. ROIs, covering one well, were created to measure total photon flux. The highest total photon flux from consecutive acquisitions was used for further analysis.

Quantification of virus and fungal titers

Serial dilutions of right lung homogenates were also used to assess the fungal load by colony-forming unit (CFU) counting. Dilutions were plated on Sabouraud agar plates and incubated at 37°C for 48 h. Reported CFU counts represent average values of duplicate plating of each dilution. DNA was extracted from lung homogenates and BAL fluid, for subsequent AsperGenius® multiplex real-time PCR assay, as previously described [32]. For influenza virus titration, serial dilutions of right lung homogenate supernatants were added to MDCK cells in quadruplicate. After 72 h incubation at 35°C, viral cytopathic effect was assessed by microscopic scoring. Virus titers were calculated by the method of Reed and Muench as log₁₀ CCID₅₀/g of lung tissue [33].

Cytokine analysis

Cytokine levels were quantified in BAL fluid and serum using an electrochemiluminescence based V-PLEX Proinflammatory Panel 1 Mouse kit from Meso Scale Diagnostics (MSD) [34].

Histopathology

Left lung 5-μm paraffin sections were cut and stained with hematoxylin-eosin and Grocott's methenamine silver staining. Staining were scored by a blinded pathologist (EV).

Statistical analysis

Statistics were performed using GraphPad Prism (version 8.1.2, GraphPad Software, San Diego, CA, USA). Longitudinal and end point data were analyzed with, respectively, two-way ANOVA or one-way ANOVA with Tukey's multiple comparisons test (repeated measurements performed from day 0 to day 4 and day 4 to day 7). All graphs represent mean values ± SD. P values are indicated in figures and are described in full in figure or figure legends and differences were considered significant if p was smaller or equal to 0.05. *P < 0.05, **P < 0.01, ***P < 0.001, ****P < 0.0001. n values represent the number of animals.

Results

Immunocompetent mice develop IPA in a background of a sublethal influenza-pneumonia

We first set out to investigate the risk of developing IPA in the setting of an influenza virus infection. To determine the effect of timing of secondary *Aspergillus* infection toward developing IAPA, mice were co-infected with conidia of a bioluminescent *A. fumigatus* strain at day 3, 4, 5, 6, or 7 post-influenza virus infection (Figure 1(a), Suppl Fig. S1). Mice infected with influenza virus alone showed moderate body weight loss and clinical worsening up to day 8 followed by recovery toward day 12 in all mice. Likewise, mice infected with only *A. fumigatus* showed limited transient body weight loss without overt clinical illness, and all these animals fully recovered. In contrast, infection with influenza virus followed by *A. fumigatus* resulted in faster and more substantial body weight loss as well as more severe clinical deterioration in some but not all mice (Figure 1(b-c)). In day 3 or day 4 co-infected fatally ill mice, histopathological examination confirmed the presence of hyphae invading the airway wall indicating airway invasive pulmonary aspergillosis which is in sharp contrast with *Aspergillus* only infected mice where only *Aspergillus* conidia were present (Figure 1(d)).

Given the observed disease severity in these mice, similarity with early IAPA development in critically ill influenza patients in ICU and therapeutic window for immune modulation in future research, in a next experiment, we zoomed in on the pathology of *Aspergillus* co-infection 3 and 4 days after influenza infection (Figure 2(a)). Consistently, these co-infected animals showed markedly faster reduced body weight as well as clinical deterioration immediately after *Aspergillus* inoculation in comparison

with influenza-only infected mice (Figure 2(b)). At day 2 post *A. fumigatus* infection, we measured extensive fungal load and high viral load (Figure 2(c-d)). In influenza- *A. fumigatus* day 4 co-infected mice, sacrificed at day 6, the cytokine profile showed a strong inflammatory burden with high levels of IL-1 β and IL-6 in BAL fluid and serum which could point toward a possible myeloid activation (Figure 2(e), Suppl Fig. S2). Furthermore, histopathology of day 4 co-infected mice exhibited severe diffuse acute purulent mainly neutrophilic bronchitis and pneumonia with epithelial erosion at day 6 (2 days post *A. fumigatus* infection) (Figure 3(a)). In contrast, single infection with influenza virus resulted in diffuse bronchiolitis with epithelial damage and multifocal lymphocytic alveolitis at day 6 (Figure 3(a)). Histopathology further confirmed the presence of *A. fumigatus* conidia with hyphae invading the airway wall in all day 4 (Figure 3(a)) and some of the day 3 co-infected mice (data not shown). Together, these data demonstrate that sublethal influenza pneumonia predisposes to airway invasive pulmonary aspergillosis in immunocompetent mice.

Oseltamivir modulates severity of influenza infection and mitigates the susceptibility to IPA in a time-dependent manner

Having established a double-hit mouse model of IAPA, we next explored the efficacy of oseltamivir in modulating the susceptibility to develop IPA. The antiviral drug was started at day 0, 2, 4 after influenza virus infection (Figure 4(a)). The non-treated day 4 co-infected mice experienced severe body weight loss by day 4, significantly worsening toward day 7, and all these animals had to be euthanized by day 8 or 9 (Figure 4(b-c)). In sharp contrast, oseltamivir initiated at day 0 or 2 generated a survival rate of 100%, in line with significantly less body weight loss and body weight recovery from day 7 onwards (Figure 4(b-c)). Also, mice treated from day 4, lost significantly less body weight loss in comparison with the non-treated group was seen toward day 7 (Figure 4(b)). Hence, oseltamivir proved highly effective the earlier the treatment was started.

We further analyzed the precise impact of oseltamivir on the severity of influenza-pneumonia through longitudinal non-invasive μ CT. Toward day 4 (during

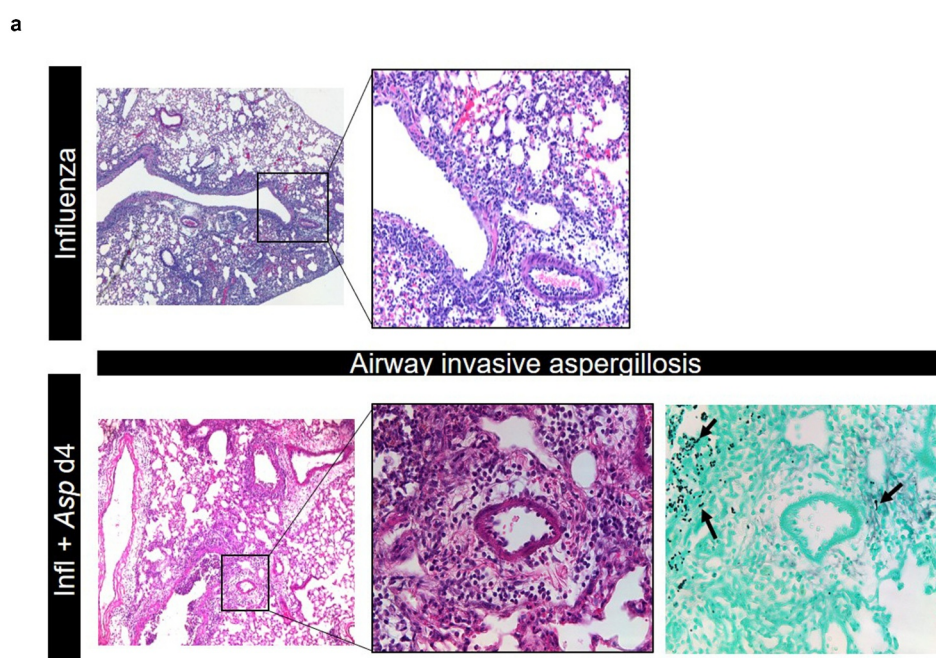


Figure 3. Histopathological confirmation of airway invasive pulmonary aspergillosis in influenza *Aspergillus* day 4 co-infected mice. (a) Hematoxylin and eosin (H&E) of left lung of (on the top) single infection with influenza virus (magnification $\times 50$, $\times 200$) showing a diffuse bronchiolitis with epithelial damage and multifocal lymphocytic alveolitis at day 6 and (on the bottom) influenza-*Aspergillus* day 4 co-infected mice sacrificed at day 6 (magnification $\times 100$, $\times 400$) showing a severe diffuse acute purulent mainly neutrophilic bronchitis and pneumonia with epithelial erosion at day 6. Grocott's methenamine silver staining (GMS) of influenza-*Aspergillus* day 4 co-infected mice sacrificed at day 6 (magnification $\times 400$). Black arrows represent hyphae invading the airway wall.

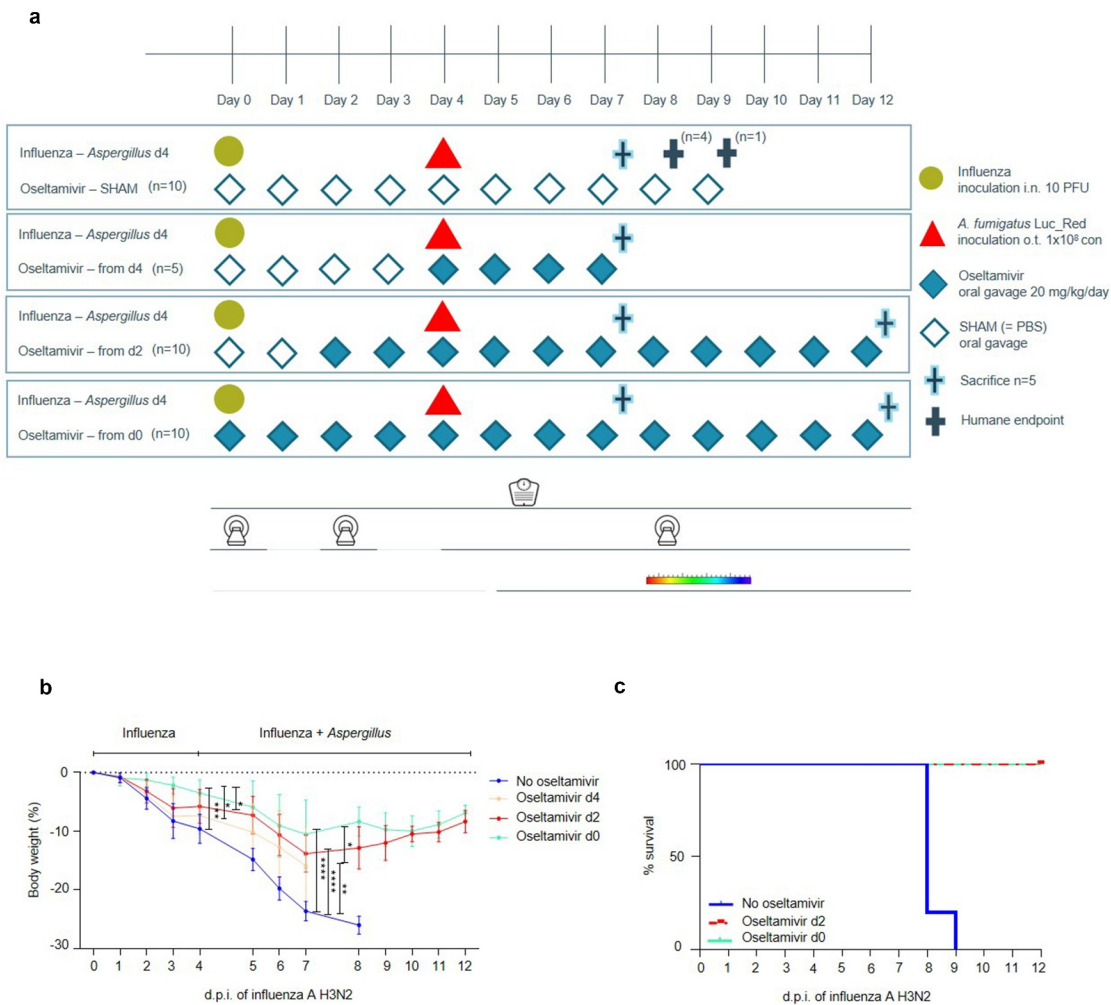


Figure 4. Osetamivir treatment improves survival and body weight reduction. (a) experimental setup of the establishment of the relationship between influenza and risk to IPA through modulation of influenza by antiviral treatment osetamivir: immunocompetent mice received influenza A on day 0, followed by inoculation with *A. fumigatus* on day 4. osetamivir (10 mg/kg) or PBS treatment twice daily by oral gavage was started at day 0 (n = 10), day 2 (n = 10) or day 4 (n = 5) up to predefined experimental endpoint (day 7 or day 12) or when humane endpoints were reached. during the experiment, mice were monitored daily (body weight, general condition, respiratory parameters) while performing micro-computed tomography (μ CT) and bioluminescence imaging (BLI). (b) Body weight evolution of immunocompetent influenza- *Aspergillus* day 4 co-infected mice without osetamivir (blue, n = 10), osetamivir treatment from day 4 (orange, n = 5), osetamivir treatment from day 2 (red, n = 10), osetamivir treatment from day 0 (green, n = 10). Longitudinal Statistical analysis: two-way ANOVA with Tukey's multiple comparisons test repeated measurements performed from day 0 until day 4 (*** p = 0,0001; * (orange, green) p = 0,0416; * p (red, green) = 0,0220) and day 4 until day 7 (**** P < 0.0001, ** p = 0,0092, * p = 0,0453) (c) Kaplan-Meier survival curve of influenza-*aspergillus* day 4 co-infected mice with no osetamivir (blue, n = 5), osetamivir treated from day 2 (red, n = 5) and osetamivir treated from day 0 (green, n = 5). all graphs are represented as mean \pm SD.

influenza infection and before *Aspergillus* co-infection), semi-quantitative scores derived from μ CT-thorax scans revealed multifocal hyperdense pulmonary lesions in the lungs of non-treated mice, while osetamivir treated mice remained largely spared from lesions development the earlier osetamivir was started (Figure 5(a-b) Suppl Fig. S3). In support of these visual observations, non-aerated lung volume, a quantitative biomarker of pulmonary infiltrates and consolidation, was markedly lower in osetamivir versus non-treated

mice (Figure 5(c)). Accordingly, the aerated lung volume was consistently higher in drug-treated animals (Figure 5(d)). Together, these results showed substantially reduced severity of influenza pneumonia the earlier the start of osetamivir treatment.

Toward day 7 (i.e. 3 days after co-infection with *Aspergillus*), we observed that osetamivir suppressed or even prevented disease exacerbation resulting from IAPA. Obvious consolidation of entire lung lobes and bronchial dilation was seen in non-treated mice

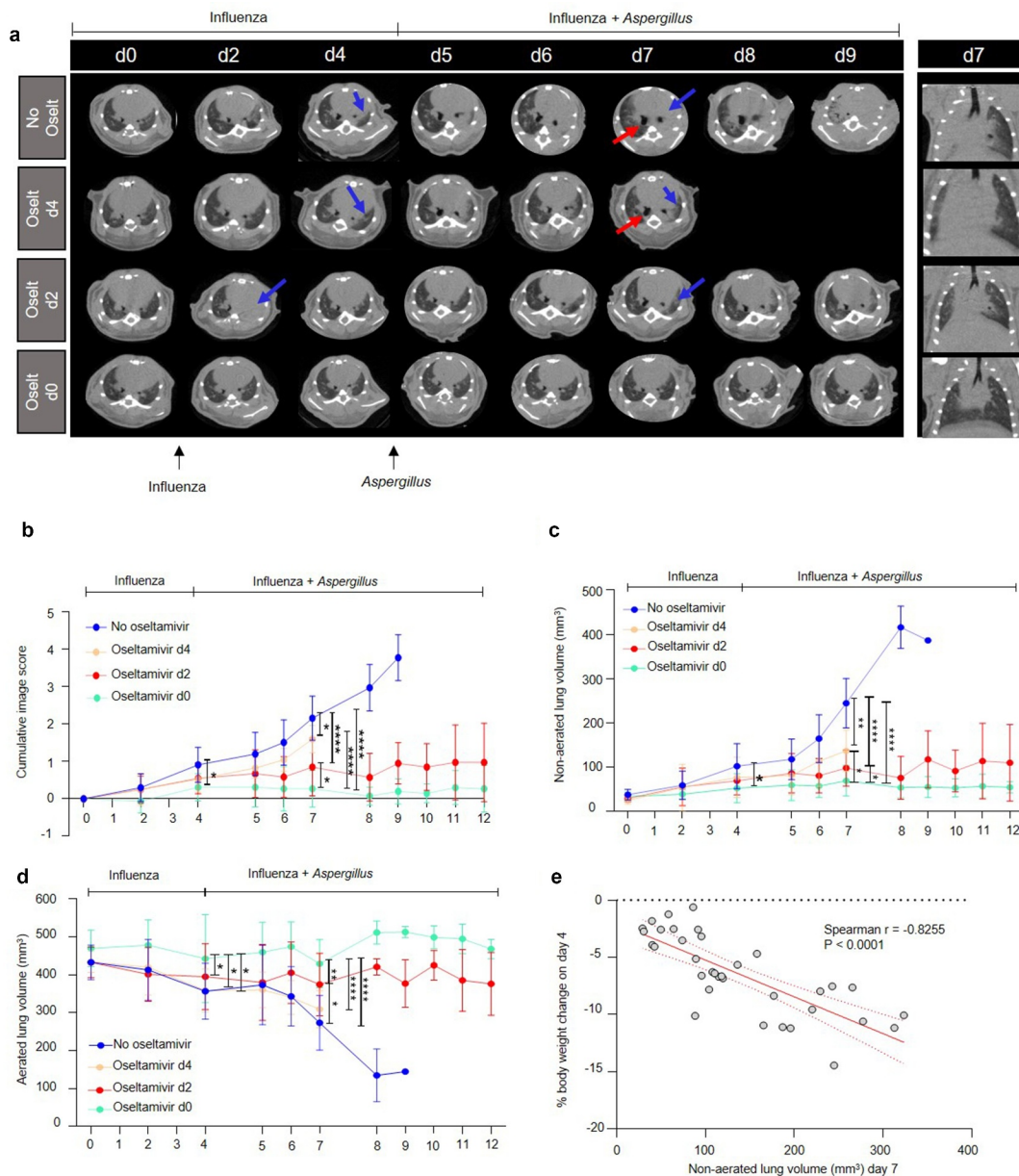


Figure 5. μ CT revealed longitudinal visualization and quantification of the disease process of IAPA and the alleviated or abolished effect from oseltamivir treatment. (a) Longitudinal transversal lung μ CT images of sham-treated (no oselt), oseltamivir treated from day 4 (oselt d4), oseltamivir treated from day 2 (oselt d2) and oseltamivir treated from day 0 (oselt d0) double-infected mice and coronal images on day 7. Blue arrow: pulmonary infiltrates, red arrow: bronchial dilation (b) Semi-quantification of image score of transverse lungs μ CT images (no oseltamivir, blue, $n = 10$; oseltamivir d4, orange, $n = 5$; oseltamivir d2, red, $n = 10$; oseltamivir d0, green, $n = 10$). Statistical analysis: two-way ANOVA with Tukey's multiple comparisons test repeated measurements performed from day 0 until day 4 (* $p = 0,0257$) and day 4 until day 7 (* (red, green) $p = 0,0158$; * (blue, orange) $p = 0,0349$; **** $P < 0.0001$) (c-d) graph represents quantification of biomarkers non-aerated lung volume (c) and aerated lung volume (d) from transverse lung μ CT images (no oseltamivir, blue, $n = 10$; oseltamivir d4, orange, $n = 5$; oseltamivir d2, red, $n = 10$; oseltamivir d0, green, $n = 10$). Statistical analysis for all longitudinal graphs: two-way ANOVA with Tukey's multiple comparisons test repeated measurements performed from day 0 until day 4 ($C = \text{non-aerated lung volume}$: * $p = 0,0388$; $D = \text{aerated lung volume}$: * (red, green) $p = 0,0359$, * (orange, green) $p = 0,0484$, * (blue, green) $p = 0,0137$) and day 4 until day 7 ($C = \text{non-aerated lung volume}$: * (orange, green) $p = 0,0106$, * (red, green) $p = 0,0185$, ** (blue, orange) $p = 0,0080$, **** $P < 0.0001$; $D = \text{aerated lung volume}$: * $p = 0,0444$, ** $p = 0,0068$, **** $P < 0.0001$). Graphs are represented as mean \pm SD. (e) Spearman correlation between % body weight change on day 4 and non-aerated lung volume on day 7. The spearman's correlation coefficient and corresponding P-value are given on the graph.

(Figure 5(a-b) Suppl Fig. S3). On the contrary, less to no pulmonary infiltrates were present in mice treated with oseltamivir, and this was more prominent the earlier treatment was started (Figure 5(a-b) Suppl Fig. S3). During *Aspergillus* co-infection (between day 4 and day 7), non-treated mice showed significant gradual increase in non-aerated and decreased aerated lung volume in comparison with treated mice (day 0 – day 2) (Figure 5(c-d)). Overall, the earlier treatment was initiated, the more significant these differences became. Although oseltamivir treated mice (day 4) do have a significantly lower non-aerated lung volume, there was no difference in aerated lung volume in comparison with non-treated mice (Figure 5(c-d)). Finally, by pooling the data from all mice, we observed that the non-aerated lung volume on day 7, strongly correlated with the body weight reduction on day 4 ($r = -0,8255$; $P < 0.0001$) (Figure 5(e)). Collectively, our analysis of lung abnormalities using imaging and μ CT-derived biomarkers demonstrated that oseltamivir modulates the severity of influenza and subsequent *Aspergillus* co-infection in a time-dependent manner during IAPA infection.

Next, we explored the impact of oseltamivir on IAPA by longitudinal follow-up of fungal burden through bioluminescence-based imaging (BLI) and microbiological gold-standard techniques. Toward day 7 (3 days post *Aspergillus* co-infection), *in vivo* bioluminescence signal intensity was lower in oseltamivir-treated conditions compared to non-treated mice; however, almost all mice elicited comparable *ex vivo* bioluminescent signal and fungal burden (CFU count) (Figure 6(a-d)). Moreover, histopathology detected clear morphological differences between treated and non-treated mice: all mice treated with oseltamivir presented with lymphocytic inflammation combined with macrophages with intracellular *A. fumigatus* conidia, whereas non-treated mice showed a diffuse acute purulent neutrophilic inflammation with *A. fumigatus* hyphae invading the airway wall (Figure 7(a), Suppl. Table. S1).

At later time points, clearance of fungal infection became increasingly evident in oseltamivir treated animals and at endpoint, CFU counts and *ex vivo* BLI signals were significantly lower (compared to non-treated), in agreement with higher Ct-values when detection was done by PCR (Figure 6(c-e)). Again, these findings nicely correlated with the histopathology since mice treated with oseltamivir from day 0 or day 2 manifested, respectively, no or only slight lymphocytic inflammation with notable signs of epithelial recovery (Figure 7(b), Suppl. Table. S1). In addition, very local or no *A. fumigatus* conidia were perceived (Figure 7

(b)). On the contrary, in non-treated mice, we observed mainly neutrophilic inflammation in bronchovesicular bundles and alveolar parenchyma with clear diffuse epithelial damage and bronchitis accompanied by *A. fumigatus* hyphae invading the airway wall (Suppl. Table. S1). Finally, mean clinical score on day 4 correlated with *ex vivo* bioluminescence on endpoint ($r = 0.6455$, $P < 0.0001$) (figure 6(f)). To conclude, early oseltamivir prevented severe lung pathology from influenza virus-*Aspergillus* co-infection and facilitated the pathogen clearing process.

Discussion

Here, we report the establishment of the first imaging-supported mouse model for the sequential interaction between influenza and *Aspergillus fumigatus*, experimentally confirming influenza as an independent risk factor for the development of IAPA in an immunocompetent host. Furthermore, we demonstrated that early oseltamivir treatment modulates the severity of influenza and mitigates the susceptibility to IAPA in a time-dependent manner. We herewith identify an early treatment to reduce the incidence of IAPA.

Until now, mouse models for influenza-associated co-infections have been limited to bacterial infections and more recently to *Cryptococcus* [35,36]. Although several clinical reports revealed influenza as an independent risk factor for IPA and a case definition of IAPA was published [1,4,5], animal models for superinfection by *Aspergillus spp.* were lacking. We provide a robust mouse model that corroborates our earlier retrospective data on IAPA in critically ill patients with severe influenza and confirm that IAPA develops in immunocompetent mice even without corticosteroids [1]. In line with the findings from Tobin *et al.* (2020) [38]. In our model, immunocompetent mice showed severe body weight loss and clinical deterioration when first infected with influenza virus and superinfected 4 days later with *A. fumigatus* conidia, whereas single infection with influenza or *Aspergillus* alone generated only transient disease. High titers of virus and fungus were present at 2 days after co-infection, pointing to an important link between high viral replication and increased susceptibility to IPA, similarly observed in other influenza models with fungal or bacterial co-infection [35,37].

Immunocompetent mice can spontaneously clear In line with the findings from Tobinet *al.* (2020) [38] *A. fumigatus conidia*, with complete restoration of lung tissue architecture, although proinflammatory cytokines, neutrophil infiltrates, *Aspergillus* conidia and CFUs were reported to be present during the first

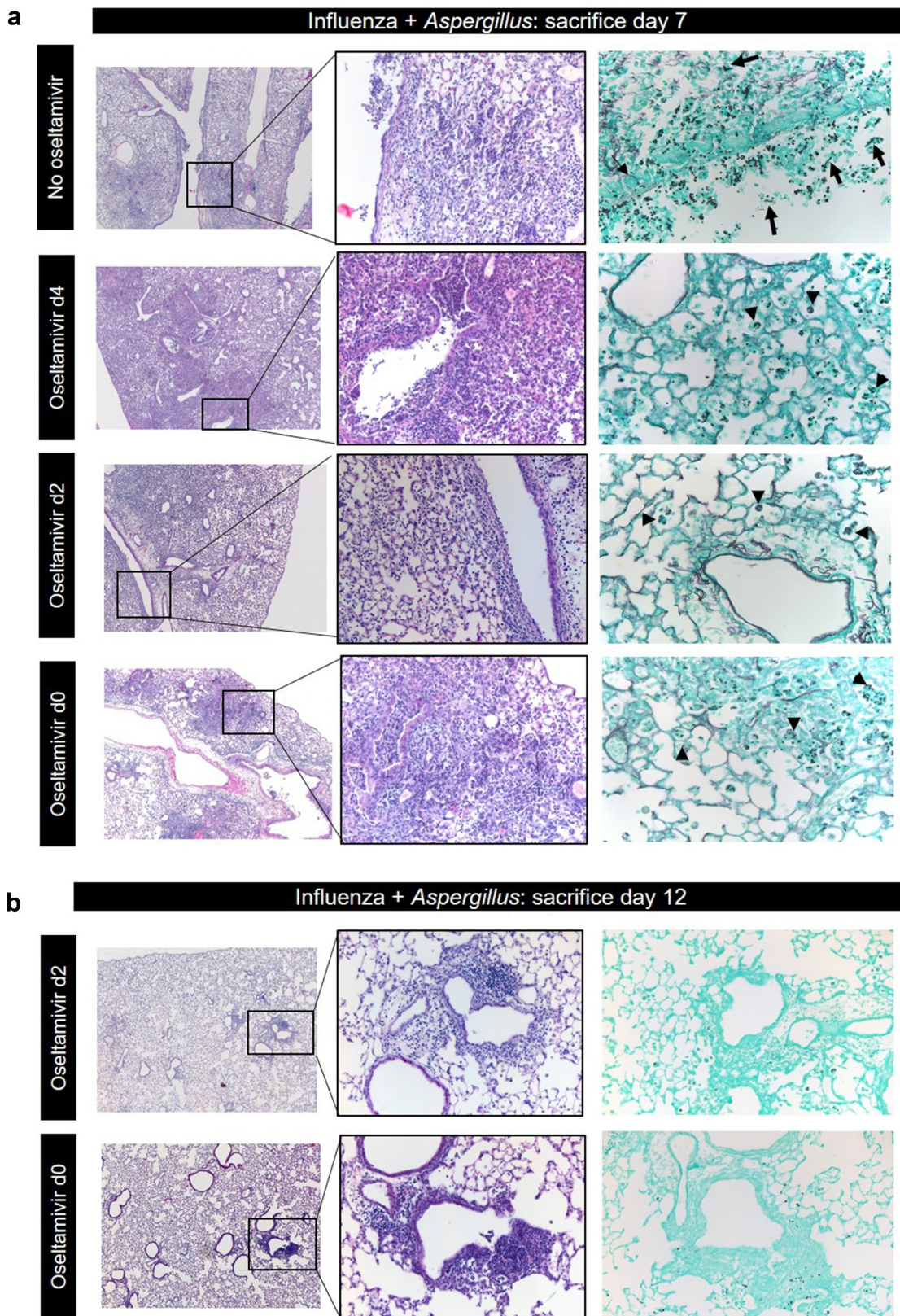


Figure 7. Oseltamivir treated mice are able to clear *A. fumigatus* in lungs. (a) Histological hematoxylin and eosin (H&E) (left, magnification $\times 50$, $\times 200$) and grocott's methenamine silver staining (GMS) (right, magnification $\times 400$) staining of left lung of different groups (no oseltamivir, oseltamivir treatment from day 4, oseltamivir treatment from day 2, oseltamivir treatment from day 0) sacrificed on day 7. Hyphae (black arrow), intracellular conidia (arrowhead). (b) Histological H&E (left, magnification $\times 50$, $\times 200$) and GMS (right, magnification $\times 200$) staining of left lung of different groups (oseltamivir treatment from day 2 and oseltamivir treatment from day 0) sacrificed on day 12.

three days of infection [39–41]. By using longitudinal imaging, we further uncovered the disease progression in co-infected mice. Notable multifocal lesions were present over the course of influenza infection, which worsened into consolidation of total lung lobes and high fungal burden after co-infection with *A. fumigatus*. Corresponding to the lesions on μ CT, severe diffuse acute purulent mainly neutrophilic bronchitis and pneumonia with epithelial erosion were discovered with histopathology. Despite the immunocompetent status, all influenza virus pre-infected mice developed proven airway invasive aspergillosis when co-infected with *A. fumigatus* on day 4, in sharp contrast to the animals infected with *A. fumigatus* only, which proved fully capable of clearing the fungus. Hence, we experimentally corroborate influenza as a strong risk factor for developing IAPA, which is independent of other immunosuppressive regimens or conditions.

There is ample evidence from clinical studies that early oseltamivir treatment improves the outcome in patients with severe influenza, by reducing the duration of hospitalization, complications, and hospital mortality [17–19,42,43]. The importance of early influenza treatment was also seen in a ferret model [44]. Likewise, oseltamivir is capable of reducing the viral load and the severity of lung infection/lung damage [20,21]. On top of this evidence, we observed that oseltamivir not only reduces the severity of influenza, but also mitigates the susceptibility to IAPA. As far as we know this has never been demonstrated so far. However, a pre-requisite is that oseltamivir started early enough. This conclusion is supported by our comprehensive clinical, radiological, pathophysiological and microbial analysis. First, early oseltamivir fully prevented the fatal outcome of IAPA. Secondly, antiviral therapy resulted in less pulmonary infiltrates, less severe influenza pneumonia and smaller lesions on μ CT after *A. fumigatus* co-infection. Thirdly, the increase in fungal burden was strongly (or even completely) inhibited in mice that received early oseltamivir. Finally, histopathological examination of lung tissue damage confirmed that the drug-treated mice were able to completely recover from this serious co-infection. To conclude, early oseltamivir administration in mice with sub-lethal influenza successfully lowers the susceptibility to develop IAPA. Our pre-clinical findings warrant future clinical studies focusing on reducing IAPA incidence, by impacting on influenza severity via oseltamivir.

Regarding *Aspergillus* clearing, we observed that oseltamivir-treated mice carried macrophages with

intracellular conidia of *Aspergillus* at 3 days after its inoculation. This concurs with an active antifungal immune response where macrophages phagocytose *Aspergillus* conidia [45]. Remarkably, we did not observe this in non-treated mice suggesting that influenza might cause some immune dysregulation, which is prevented by early treatment with oseltamivir. Influenza is known to induce a strong IFN- γ /Th1 response decreasing the macrophage phagocytic activity in an influenza/*Streptococcus pneumoniae* model secondary to a downregulation of a scavenger molecule (MARCO) at the cell surface [15]. Considering the histology findings in our model, the latter hypothesis could be appropriate with a severe reduction in phagocytic properties in mice co-infected with influenza and *A. fumigatus* while this phagocytic function could be restored once the viral burden decreases after oseltamivir treatment. However, our observations argue for a more comprehensive study. The transient presence of *Aspergillus* conidia inside macrophages also provides an explanation for why bioluminescence signals and CFU counts were positive yet consistently low on day 7, but negative on day 12. Thus, oseltamivir treatment reduces the severity of the infectious pathology and drives/facilitates an active antifungal clearing process.

Importantly, the timing of oseltamivir treatment remains essential. Early treatment reduces influenza disease symptoms accompanied by a decreasing risk of acquiring IAPA. However, once IAPA is present, it is not clear whether neuraminidase inhibition is beneficial or detrimental. There is evidence that blocking neuraminidase activity in a murine model of aspergillosis is detrimental [46,47]. Blocking neuraminidase might have a negative impact on anti-*Aspergillus* host defense itself [48–50]. However, our results show that this possibly negative effect on the fungal host response will probably be balanced out by the positive effect on influenza.

In conclusion, we established the first successful preclinical imaging-supported double-hit mouse model of IAPA. This model recapitulates and confirms influenza as a risk factor for the development of invasive and potentially fatal pulmonary aspergillosis. We demonstrated that early oseltamivir treatment mitigates the risk to develop IAPA. Besides reinforcing the recommendation to start oseltamivir as soon as possible (within 48–72 h) in case of severe influenza our findings indicate that early onset of oseltamivir might also reduce the high mortality and morbidity associated with IAPA [1]. In a broader context, this double-hit mouse model is the key for future research aimed at unraveling the underlying immune mechanism of IAPA.

Acknowledgments

The authors would like to thank Ria Van Berwaer for fine technical assistance. All preclinical imaging was performed in the Molecular Small Animal Imaging Center (MoSAIC), a KU Leuven core facility. This work was supported by the [Research Foundation Flanders (FWO), project funding] under Grants [1506114N, G053121N, G057721N] to [GVV, JW, SHB and KL]; [clinical research funding] to [JW], [Research Foundation Flanders (FWO), aspirant mandate] under Grant [1186121N] to [LS] and [11E9819N] to [LV]; [KU Leuven internal funds] under Grant [C24/17/061] to [GVV] and [VIDI grant from ZonMW] to [FvdV].

Disclosure statement

No potential conflict of interest was reported by the author(s).

Funding

This work was supported by the Flemish Research Foundation (FWO) [1506114N, 11E9819N, G053121N, G057721N, 1186121N] and KU Leuven internal funds [C24/17/061].

Authorship contributions

LS, LV, AF, ARS, CJ, BL, TO and MB performed experiments; LS, LV, BL, TO, EV and GVV analyzed data; KL, GVV supervised the experiments and data analysis; LS, LV, KL, JW, and GVV designed the study; LS and LV wrote the first manuscript draft; ARS, LN, MB, FVV, SHB, KL, JW and GVV reviewed the manuscript; and all authors approved the final version of the manuscript.

Data availability statement

Data is available upon request.

ORCID

Laura Selde-slachts  <http://orcid.org/0000-0002-9562-2923>
Greetje Vande Velde  <http://orcid.org/0000-0002-5633-3993>

References

- [1] Schauwvlieghe AFAD, Rijnders BJA, Philips N, et al. Invasive aspergillosis in patients admitted to the intensive care unit with severe influenza: a retrospective cohort study. *Lancet Respir Med* [Internet]. 2018;6(10):782–792.
- [2] Wei-Lun L, Wen-Liang Y, Khee-Siang C, et al. Aspergillosis related to severe influenza : a worldwide phenomenon? *Clin Respir J*. 2019 March;13(8):540–542.
- [3] Van De Veerdonk FL, Kolwijck E, Lestrade PPA, et al. Influenza-associated aspergillosis in critically ill patients. *Am J Respir Crit Care Med*. 2017;196(4):524–527.
- [4] Vanderbeke L, Spriet I, Breynaert C, et al. Invasive pulmonary aspergillosis complicating severe influenza: epidemiology, diagnosis and treatment. *Curr Opin Infect Dis*. 2018;31(6):471–480.
- [5] Verweij PE, Rijnders BJA, Rjm B, et al. Review of influenza-associated pulmonary aspergillosis in ICU patients and proposal for a case definition: an expert opinion. *Intensive Care Med* [Internet]. 2020;(Cdc). 10.1007/s00134-020-06091-6
- [6] Principi N, Camilloni B, Alunno A, et al. Drugs for Influenza Treatment: is There Significant News? *Front Med*. 2019 May;6:1–7.
- [7] World Health Organization Influenza (Seasonal) [Internet]. 2019/2018 Nov 6 [cited 2021 Jan 14]. Available from: [https://www.who.int/news-room/fact-sheets/detail/influenza-\(seasonal\)](https://www.who.int/news-room/fact-sheets/detail/influenza-(seasonal))
- [8] Paget C, Trottein F. Mechanisms of bacterial superinfection post-influenza: a role for unconventional T cells. *Front Immunol*. 2019 MAR;10. 10.3389/fimmu.2019.00336.
- [9] Herold S, Becker C, Ridge KM, et al. Influenza virus-induced lung injury: pathogenesis and implications for treatment. *European Respiratory Journal*. 2015;45(5):1463–1478.
- [10] Rynda-Apple A, Robinson KM, Alcorn JF. Influenza and bacterial superinfection: illuminating the immunologic mechanisms of disease. *Infect Immun*. 2015;83(10):3764–3770.
- [11] Mina MJ, Klugman KP. The role of influenza in the severity and transmission of respiratory bacterial disease. *Lancet Respir Med* [Internet]. 2014;2(9):750–763.
- [12] Beumer MC, Koch RM, van Beuningen D, et al. Influenza virus and factors that are associated with ICU admission, pulmonary co-infections and ICU mortality. *J Crit Care* [Internet]. 2019;50:59–65.
- [13] McCullers JA. The co-pathogenesis of influenza viruses with bacteria in the lung. *Nat Rev Microbiol*. 2014;12(4):252–262.
- [14] Sun K, Metzger D. Influenza infection suppresses NADPH oxidase-dependent phagocytic bacterial clearance and enhances susceptibility to secondary MRSA infection. *J Immunol*. 2015;192(7):3301–3307.
- [15] Sun K, Metzger DW. Inhibition of pulmonary antibacterial defense by interferon- γ during recovery from influenza infection. *Nat Med*. 2008;14(5):750–763.
- [16] Villeret B, Solhonne B, Straube M, et al. A Virus Pre-Infection Exacerbates *Pseudomonas aeruginosa*-Mediated Lung Damage Through Increased MMP-9 Expression, Decreased Elafin Production and Tissue Resilience. *Front Immunol*. 2020 (February);11:1–15.
- [17] Hernu R, Chroboczek T, Madelaine T, et al. Early oseltamivir therapy improves the outcome in critically ill patients with influenza: a propensity analysis. *Intensive Care Med*. 2018;44(2):257–260.
- [18] Lee N, Ison M. Neuraminidase inhibitors for influenza-like illness in primary care. *Lancet* (London, England) [Internet]. 2019;6736(19):10–11. <http://www.ncbi.nlm.nih.gov/pubmed/31839278>

- [19] Butler CC, van der Velden AW, Bongard E, et al. Oseltamivir plus usual care versus usual care for influenza-like illness in primary care: an open-label, pragmatic, randomised controlled trial. *Lancet* (London, England) [Internet]. 2019;6736(19):1–11. Available from <http://www.ncbi.nlm.nih.gov/pubmed/31839279>
- [20] Smee DF, Barnard DL, Jones SM, Activities of JNJ63623872 and oseltamivir against influenza A H1N1pdm and H3N2 virus infections in mice. *Antiviral Res* [Internet]. 2016;136:45–50.
- [21] Zarogiannis SG, Noah JW, Jurkuvenaite A, et al. Comparison of ribavirin and oseltamivir in reducing mortality and lung injury in mice infected with mouse adapted A/California/04/2009 (H1N1). *Life Sci* [Internet]. 2012;90(11–12):440–445. Available from.
- [22] McCullers JA. Effect of antiviral treatment on the outcome of secondary bacterial pneumonia after influenza. *J Infect Dis*. 2004;190(3):519–526.
- [23] McCullers JA. Preventing and treating secondary bacterial infections with antiviral agents. *Antivir Ther*. 2011;11(C):128–137.
- [24] McCullers JA, Bartmess KC. Lethal synergism between influenza virus and *Streptococcus pneumoniae*. *J Infect Dis*. 2003;187(10):1674–1675.
- [25] Ikeda S, Neyts J, Verma S, et al. In vitro and in vivo inhibition of ortho- and paramyxovirus infections by a new class of sulfonic acid polymers interacting with virus-cell binding and/or fusion. *Antimicrob Agents Chemother*. 1994;38(2):1674–1675.
- [26] Fleck CB, Brock M. *Aspergillus fumigatus* catalytic glucokinase and hexokinase: expression analysis and importance for germination, growth, and conidiation. *Eukaryot Cell*. 2010;9(7):1120–1135.
- [27] Zaehle C, Gressler M, Shelest E, et al. Terrein biosynthesis in *aspergillus terreus* and its impact on phytotoxicity. *Chem Biol* [Internet]. 2014;21(6):719–731.
- [28] Poelmans J, Himmelreich U, Vanherp L, et al. A Multimodal Imaging Approach Enables In Vivo Assessment of Antifungal Treatment in a Mouse Model of Invasive pulmonary aspergillosis. 2018;1–13.
- [29] Berghen N, Dekoster K, Marien E, et al. Radiosafe micro-computed tomography for longitudinal evaluation of murine disease models. *Sci Rep*. 2019;9(1):1–10.
- [30] Vande Velde G, Poelmans J, De Langhe E, et al. Longitudinal micro-CT provides biomarkers of lung disease that can be used to assess the effect of therapy in preclinical mouse models, and reveal compensatory changes in lung volume. *DMM Dis Model Mech*. 2016;9(1):91–98.
- [31] Poelmans J, Hillen A, Vanherp L, et al. Longitudinal, in vivo assessment of invasive pulmonary aspergillosis in mice by computed tomography and magnetic resonance imaging. *Lab Investig*. 2016;96(6):692–704.
- [32] Chong GM, van der Beek MT, von dem Borne PA, et al. PCR-based detection of *Aspergillus fumigatus* Cyp51A mutations on bronchoalveolar lavage a multicentre validation of the AsperGenius assay® in 201 patients with haematological disease suspected for invasive aspergillosis. *J Antimicrob Chemother*. 2016;71(12):3528–3535.
- [33] Reed L, Muench H. A simple method of estimating fifty per cent endpoints. *Am J Epidemiol*. 1938;27(3):493–497.
- [34] Garcia-Perez JE, Mathé L, Humblet-Baron S, et al. A framework for understanding the evasion of host immunity by *Candida* biofilms. *Front Immunol*. 2018;9(MAR):1–8.
- [35] Oliveira LVN, Costa MC, TFF M, et al. Influenza a virus as a predisposing factor for cryptococcosis. *Front Cell Infect Microbiol*. 2017;7(SEP):1–13.
- [36] Moorthy AN, Narasaraju T, Rai P, et al. In vivo and in vitro studies on the roles of neutrophil extracellular traps during secondary pneumococcal pneumonia after primary pulmonary influenza infection. *Front Immunol*. 2013 March;4:1–13.
- [37] Müller HE. Lethal Synergism between Influenza Virus and *Streptococcus pneumoniae*. *J Infect Dis*. 2003;187(10):1674.
- [38] Tobin JM, Nickolich KL, Ramanan K, et al. Influenza Suppresses Neutrophil Recruitment to the Lung and Exacerbates Secondary Invasive Pulmonary Aspergillosis. *J Immunol*. 2020;205(2):1674.
- [39] Malacco NLSO, Souza JAM, Mendes AC, et al. Acute lung injury and repair induced by single exposure of *Aspergillus fumigatus* in immunocompetent mice. *Future Microbiol*. 2019;14(17):480–488.
- [40] Cenci E, Mencacci A, Fe C, et al. Cytokine- and T helper – dependent lung mucosal immunity in mice with invasive pulmonary aspergillosis. *J Infect Dis*. 1998;178(6):471–480.
- [41] Brieland JK, Jackson C, Menzel F, et al. Cytokine networking in lungs of immunocompetent mice in response to inhaled *aspergillus fumigatus*. *Infect Immun*. 2015;69(3):1554–1560.
- [42] Dobson J, Whitley RJ, Pocock S, et al. Oseltamivir treatment for influenza in adults: a meta-analysis of randomised controlled trials. *Lancet*. 2015;385(9979):1729–1737.
- [43] Muthuri SG, Venkatesan S, Myles PR, et al. Effectiveness of neuraminidase inhibitors in reducing mortality in patients admitted to hospital with influenza A H1N1pdm09 virus infection: a meta-analysis of individual participant data. *Lancet Respir Med*. 2014;2(5):395–404.
- [44] Govorkova EA, Ilyushina NA, Boltz DA, et al. Efficacy of oseltamivir therapy in ferrets inoculated with different clades of H5N1 influenza virus. *Antimicrob Agents Chemother*. 2007;51(4):1414–1424.
- [45] Luther K, Rohde M, Sturm K, et al. Characterisation of the phagocytic uptake of *Aspergillus fumigatus* conidia by macrophages. *Microbes Infect*. 2008;10(2):175–184.
- [46] Dewi IMW, Cunha C, Jaeger M, et al. Neuraminidase and SIGLEC15 modulate the host defense against pulmonary aspergillosis. *Cell Reports Med*. 2021;2(5):5.

- [47] Dewi I, Cunha C, Vanderbeke L, et al. Oseltamivir affects host defense against invasive pulmonary aspergillosis. Paper presented at: 28th ECCMID; 2018 Apr 21-24; Madrid, Spain.
- [48] Revilla N, Corral J, Miñano A, et al. Multirefractory primary immune thrombocytopenia; targeting the decreased sialic acid content. *Platelets* [Internet]. 2019;30(6):743–751.
- [49] Shao L, Wu Y, Zhou H, et al. Successful treatment with oseltamivir phosphate in a patient with chronic immune thrombocytopenia positive for anti-GPIb/IX autoantibody. *Platelets*. 2015;26(5):495–497.
- [50] Bigot P, Auffret M, Gautier S, et al. Unexpected platelets elevation in a patient with idiopathic thrombocytopenia treated with oseltamivir for influenza infection. *Fundam Clin Pharmacol*. 2016;30(5):483–485.